

# EXPERIMENTAL INVESTIGATION OF EJECTA GENERATED BY THE HYPERVELOCITY IMPACT OF ALUMINUM PROJECTILES ON CONTINUOUS AND MESH BUMPERS

N.N. Myagkov<sup>(1)</sup>, L.N. Bezrukov<sup>(2)</sup>, T.A. Shumikhin<sup>(1)</sup>

<sup>(1)</sup>*Institute of Applied Mechanics of RAS, Russia, 119991, Moscow, Leninskiy pr. 32a, Email: nn\_myagkov@mail.ru*

<sup>(2)</sup>*FGUP GosNIIAS, Russia, 125319, Moscow, ul. Victorenko, 7, Email: bezrukov@gosniias.ru*

## ABSTRACT

Ejecta particles generated at the impact of a micrometeoroid or space debris particle on the element of a spacecraft in orbit may pose a serious damage threat to other spacecraft structures and increase the common level of space debris pollution. We studied experimentally the dependence of ejecta mass on the parameters of aluminum plates and steel meshes. The ejecta particles were caught by polystyrene foam and then recovered. A microscope analysis and weighting of the recovered particles were made, and the spatial distribution of their trajectories was rendered. The model of destruction of an ejecta cone is evaluated to explain the effect of the formation of jets in the ejecta cone, and to estimate the total number of the jets.

## 1. INTRODUCTION

The hypervelocity impact of a particle on a target is accompanied by a sufficient ejection of material in the semi-space from which the particle approached towards the target. This ejected material is called ejecta. The total mass of the ejecta may be higher than the mass of the particle. In the case of the hypervelocity collision of such a particle, being an element of space debris or a meteoroid, with a spacecraft, the emission of the ejecta results in the further pollution of the outer space, enlarging population of artificial micro-particles. On the other hand, the emitting ejecta particles, possessing considerable velocities, may present hazard to onboard installed facilities. In any case the phenomena of ejecta occurred in orbit may be regarded as a negative event resulting in worsening of the common conditions for reliable functioning of artificial satellites and spacecrafts.

In view of that fact that the event of such an in-orbit collision is unpredictable and unavoidable (at least at the current stage of technological development), the only way to lessen its negative consequences is to undertake some preliminary measures aimed either on elimination of totally emitted ejecta, or on positioning of outside installed devices, which may be sensible to ejecta, with regard to possible ejecta trajectories of propagation. Despite the abundance of existing experimental data on the properties of ejecta, both these issues reveal the necessity for detailed study of the materials which are used for spacecraft construction. Total mass of ejecta particles, the

distribution of their sizes, velocities, and directions – all that characteristics are of interest. Beyond any doubts, an extended data-base accumulating results of many experiments would be a good help for the contribution into existing models describing the evaluation of space debris in-orbit population and for the improvement and evaluation of the ejecta models as well.

The experiments that were conducted aimed to the study of ejecta knocked out thin aluminium plates and steel meshes by an aluminium sphere. The choice of the targets was predicted by the fact that these materials are used as for constructional purpose and as elements of meteoroid and space debris shielding, yet the comparison between the ejecta from continuous and discontinues bumpers seems to be also of significant interest. The idea was to catch ejecta particles using a collector made of low-density substance. Out of practical reasons, we took polystyrene foam as the material for the collectors. This foam can be easily processed and dissolved by means of ordinary solvents.

## 2. EXPERIMENTAL SET-UP

All experiments were conducted using a two-stage light gas gun installed in the FGUP GOSNIIAS. The common scheme of the experiments is as follow. A two-stage light-gas gun accelerates the sabot with a projectile fixed in it. In the expansion chamber connected with the second-stage barrel the projectile is detached from the sabot with the help of the couple of steel disk-shaped cutters. Then the projectile arrives into the target chamber where its velocity is registered by the contact-type velocimeter. Beyond the velocimeter the collector is installed with the attached target. The pressure in the system after the evacuation of air was no more than 20% of the normal atmospheric pressure.

In all experiments a 6.35mm aluminium sphere was used as a projectile. The range of impact velocities was 2.2-3.2 km/s; the impact was normal to a target. For the targets we used 1.45 and 3.0mm thick aluminium (D-16 and AMg6 respectively) plates; three staked together 1.0x0.32mm steel meshes (1.0mm – the diameter of the mesh wire and 0.32mm is the gape between two neighbouring wires in the mesh) and a single 2.0x1.0mm steel mesh. All experiment data are provided in Tab. 1.

Collectors were made of  $15\text{kg/m}^2$  polystyrene foam (commercial brand mark PSB-S15). The collector had a cylindrical form and consisted of two parts (Fig 1.) The frontal part was covered by a protective plate to prevent the damage of the collector by shot-debris. Along the symmetry axis of the collector a 40mm channel was made to provide projectile entering. Also the hole was made in the frontal protective plate. The impact of the projectile on the target attached to the rear part of the collector led to the emission of ejecta particles into the camera of the collector where they, having penetrated into the low-density collector material, were captured leaving visible traces of penetration on the camera surface.

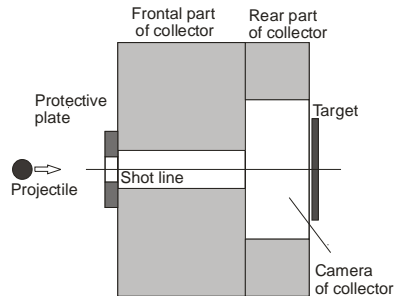


Figure 1. Scheme of a foam collector (cross-section along the shot-line). The thickness of the frontal part is 100mm, of the rear part is 50mm. The external diameter of the collector is 250mm; the internal diameter of the frontal part is 40mm; the diameter of the camera is 110mm (150mm in some experiments)

A foam collector was put into a metal cylindrical shell (Fig. 2). The full assembly was installed in the target chamber. The special measures were undertaken to assure an accurate aiming providing the coaxiality of the assembly axis with the shot-line which, taking into account the limited size of the collector, is a quite crucial point for the favourable symmetrical distribution of ejecta particles over the collector camera. One important point to add is that the collector geometry was chosen to provide that the main mass of the ejecta forming so called ejecta cone at the angle about 60 degree taken from the target would be captured by the thick frontal part of the collector, whereas the ejecta knocked out at higher angles, by the rear part.



Figure 2. The rear view of a collector with an attached aluminium plate target

To extract the captured ejecta particles we used some available solvents. The extracted particles were weighted using the electronic laboratory balance

(with accuracy up to 0.5mg). The recovered substance was also studied using a metallurgical microscope.

A part of collectors were cut into five slices each perpendicularly to the collector axis with the aim of getting information about distribution of traces which were left inside the foam by the ejecta particles. The slices were scanned using digital scanner.

### 3. EXPERIMENT RESULTS

Selected experiments are presented in Tab. 1a-1b.

#### 3.1 Mass of recovered particles

The ejecta particles were recovered for shots 1- 6.

The external appearance of collector camera surfaces for shot 1 made on the 1.45mm aluminum plate is as follow. The most intensive flow of ejecta particles in shot 1 is distributed along the circle of diameter 120mm according the traces on the back side of the frontal part of the collector (Fig. 3), which reflects a cone shape of the flow with the generating line of the cone making an angle about 50 degree from the shot line. The circumference distribution of particles in the cone-flow is quite heterogeneous (Fig. 3). It reveals six zones of concentration of particles.



Figure 3. Rear side of the frontal part which was faced to the target (shot 1)

For the purpose of detailed analysis the frontal and rear parts of the collector were cut on six sectors according the zones of concentration. That allowed to perform convenient visual inspection of the side walls of the collector camera (Fig.4) and recover the particles from each individual sector as well. Some amount of particles was knocked out the target surface at grater angles according the imprint of the thread-like vertical traces (Fig.4) on the side wall of the collector camera.



Figure 4. Part of the side wall of the collector camera. The target was placed upwardly relatively the photo (shot 1). The horizontal size is 60 mm.

The weight of recovered particles for twelve pieces of the collector (six for frontal and six for rear part) listed in Tab. 2. The number of quite large aluminum particles (more than 0.5mm in size), which was counted up visually, correlates though with the evaluated weight of substance for each sector (Tab. 2), which prove reliability of considered estimation.

The particles recovered from collectors were studied using a microscope (Fig.5). The composition of the extracted substance includes:

- large aluminum particles (up to 0.5mm in size) (#1 in Fig. 5);
- fine aluminum particles of gray colour (#2 in Fig. 5); particularly, this particles were found in abundance on the internal wall of the channels made by the ejecta in the collector foam
- aluminum spheres of size up to  $50 \mu$  which obviously were formed obviously due to the melting of projectile and target material (#3 in Fig. 5)
- glass spheres of size up to  $20 \mu$  (#4 in Fig. 10); they enter into the composition of a composite material used for the fabrication of a sabot

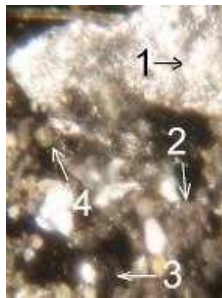


Figure 5. Recovered substance (magnification  $\times 100$ )

The ejecta from shot 4 generated at impact on 3 stacked together steel meshes was recovered. The mass of the ejecta from this shot and from two other shots 5 and 6 occurred to be sufficiently lower than from impacts on an aluminum plate (Tab. 1a). The reaction of the recovered dust on magnetic field reveals the presence of iron. This iron dust seems to be consisted of the finest ejecta particles knocked-out from the steel mesh.



Figure .6 Collector camera (shot 4)

The exterior appearance of the collector surface (Fig. 6) differs from the one of shot 1 (Fig. 3), which was

made at the aluminum plate. The surface of the collector camera is visually clean. There are no traces of inlet holes made by ejecta.

### 3.2 Ejecta particle trajectories

The ejecta from the impact on a 3mm-thick aluminum plate occurred to be quite intensive. That led to the formation of prolonged channels in collectors (up to 100mm in length and up to several millimeters in width). Assuming that the particle trajectories are not affected by the event of particles contact with collector material, the direction of channels can be used for estimation of the angles at which the particles leave the target. For this purpose thin metal probes were used (fig. 7) and the following parameters were estimated:  $d_c$  - the distance between two opposite craters situated on the imaginary formed as intersection of an ejecta-cone and the plane of the collector rear surface,  $d_b$  - a diameter of the circle formed as intersection of an ejecta-cone and the plane of the target,  $\alpha_I$  - the angle between the trajectory of channel I and the surface of the collector ( $\alpha_{II}$  - an angle, consequently, for channel II). The angle  $\alpha$  helps calculate the angle  $\varphi$  between the particle trajectory and the shot-line.

The retrieved parameters for shot 7 are presented in Tab. 3. The parameters reveal quite inhomogeneous distribution of the angle  $\varphi$ .

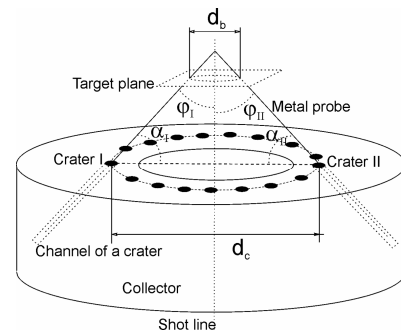


Figure 7. Scheme of particle trajectories measurement

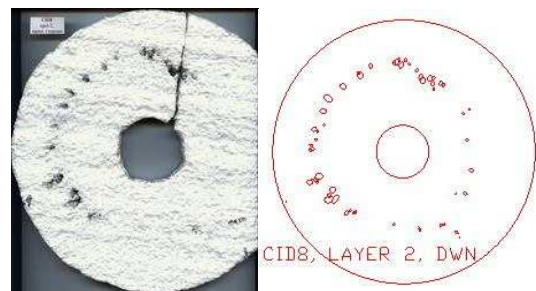


Figure 8. Photo of down-range surface (second layer) and its digital image (shot 8).

Also the trajectories were estimated as follow. Some of the available collectors were cut into five 20 mm thick layers perpendicularly to the shot-line. The images of the layer surfaces were digitally processed.

The processing consisted in approximation of each hole observed on a layer by an ellipse. Fig.8 shows the image of the down-range surface of the second collector layer form shot 8 with, and presents its digital pattern obtained by the image processing.

Obtained data allow rendering distribution of ejecta particles inside a collector as it is shown in Fig. 9 which presents data for shot 8.

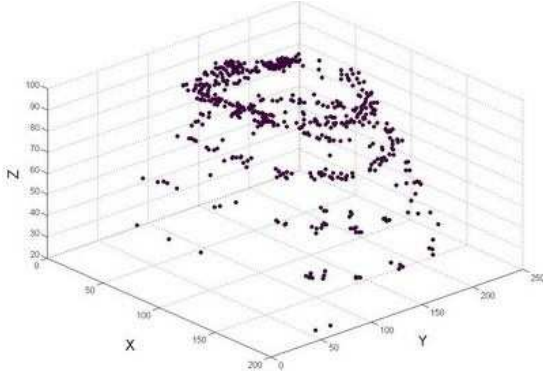


Figure 9. Spatial distribution of the channels in the collector from shot 8, (mm)

#### 4. MODEL OF EJECTA DESTRUCTION

In [1] Grady proposes as model of dynamical fragmentation is which the size of an average fragments is determined by the balance between kinetic energy and the energy of surfaces appearing at the act of fragmentation. The sufficient preposition of this model is that it is only the kinetic energy  $T$  which is taken relatively to the center of mass of an expected fragment acts in the process of fragmentation. In addition, the kinetic energy of the fragment center of mass  $T_{cm}$  is constant during the fragmentation. If the body does not expand, the local kinetic energy  $T=0$ . The improved model of dynamical fragmentation, based on the balance of energy, assumes that the elastic energy of the fragment and the local kinetic energy both contribute in generation of new fracture surfaces [2, 3]. One additional condition is that the fracture occurs only if stresses reach the critical value  $\sigma_*$ .

Let us consider the movement of the ejecta cone layer of ejecting material around the crater (Fig.10). The presence of the velocity radial component  $V_0 \cos \alpha$ , where  $V_0$  – the velocity of material in the cone and  $\alpha$  – the angle taken from target surface, eventually results in the destruction of the material. It is obvious that the velocity  $V_0$  of the material remains constant up to the event of destruction. We assume, also, that the thickness of ejected layer is small relative to the crater radius  $r_0$ . Now, we mark out a thin ring layer with radius  $r$  in the cone and consider the segment of this ring with a middle line of length  $2a$  and cross-section area equal to  $\delta S$  (Fig.11). This segment is supposed to split off finally from the ring forming two new surfaces with total area equal to  $2\delta S$ .

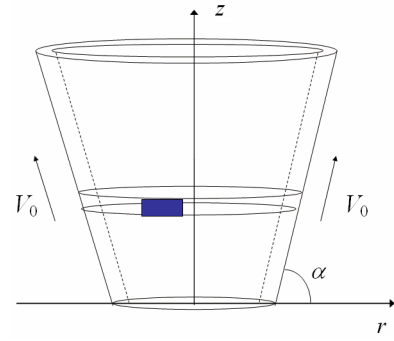


Figure 10. Ejecta cone with a ring layer and a sector of this layer.  $\alpha$  - angle taken from target,  $V_0$  – constant velocity of material in the layer

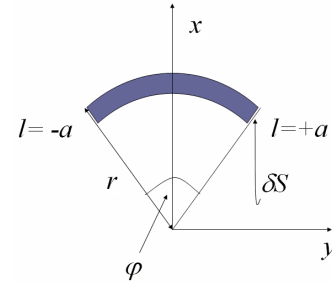


Figure 11. Segment of the layer:

$l$  – distance along the middle line,  $-a \leq l \leq +a$ ,  $r$  – radius of ejecta,  $\delta S$  -area of the cross-section of the ring layer,  $\varphi$  - angular coordinate ( $\varphi=0$  corresponds to  $l=0$  and  $\varphi \in [-\varphi^*/2; +\varphi^*/2]$ ,  $\varphi^*/2 = a/r$ )

We assume that the destruction on the both ends of the segment occurs simultaneously and similarly. The successive detachment of the rings, to which we divide imaginary the ejecta cone, results in splitting of this cone on jets. The evaluation of the average value of  $2a$  allows us to estimate the number of jets.

Under the assumed prepositions the coordinates and velocity of the center of mass of the segment (Fig.11) are:

$$y_c = 0; \quad x_c = \frac{\sin(a/r)}{a} r^2,$$

$$V_{y,c} = 0; \quad V_{x,c} = \frac{\sin(a/r)}{a} r V_0 \cos \alpha$$

The local kinetic energy of the segment, taken relatively to its center of mass is:

$$T = \rho \delta S (V_0 \cos \alpha)^2 r^2 \left( \left( \frac{a}{r} \right)^2 - \sin^2 \left( \frac{a}{r} \right) \right) \quad (1)$$

For the case  $a \ll r$  using Eq. 1 we get:

$$T = \frac{1}{3} \rho \delta S (V_0 \cos \alpha)^2 \frac{a^3}{r^2} \quad (2)$$

where  $\rho$  - is the density of the ejecting material. We assume that the destruction of the ring occurs at small deformation. For the specific elongation  $\delta_i$  at which

the destruction of the material takes place in Eqs. 1-2 we can put  $r$  as follow

$$r \approx r_0(1 + \delta_l) \quad (3)$$

where  $r_0$  is the radius of the base of the ejecta cone.

The deviation of surface energy which occurs because of the generation of two new surfaces on the segments edges is:

$$\Gamma = 2\gamma\delta S = \delta S \frac{K_C^2}{\rho c_0^2} \quad (4)$$

where  $\gamma$  is density of surface energy and  $K_C$  is a critical stress intensity factor at a plane stress state. Following [2] let us assume that the deviation of elastic energy is not sufficient in the energy balance. Therefore, taking that the whole local kinetic energy is used for generation of new fracture surfaces we have that  $T=\Gamma$  and from Eqs. 1-4 we get that

$$\rho(V_0 \cos \alpha)^2 \frac{r^2}{a} \left( \left( \frac{a}{r} \right)^2 - \sin^2 \left( \frac{a}{r} \right) \right) = \frac{K_C^2}{\rho c_0^2} \quad (5)$$

or, if  $a \ll r$ :

$$\frac{1}{3} \rho(V_0 \cos \alpha)^2 \frac{a^3}{r^2} = \frac{K_C^2}{\rho c_0^2} \quad (6)$$

From Eq. 6 the characteristic size of the segment which remains after the destruction of the ring can be evaluated in an explicit form:

$$2a = 24^{1/3} \left( \frac{K_C r}{\rho c_0 V_0 \cos \alpha} \right)^{2/3} \quad (7)$$

The elastic energy of the considered segment is

$$P = \frac{1}{2} \frac{(\sigma_*)^2}{E} 2a\delta S \quad (8)$$

where  $E$  is Young's modulus,  $\sigma_*$  is the critical stress at which the destruction occurs. Taking into account the elastic energy we get the balance of energy in the form  $T+P = \Gamma$  [2]. The estimate shows that at ejection velocities  $V_0 > 0.5$  km/s the local kinetic energy of the segment is sufficiently higher than its elastic energy.

Now let us estimate how the characteristic size of the zone of the ejecta destruction depends on the ejecta velocities  $V_0$ . The data for aluminum are presented in Tab. 4. The angle  $\alpha$  is equal approximately  $60^\circ$ . The radius of ejecta cone at its base  $r_0$  taken from shot 7 is about 11mm. The evaluation made with Eq. 5 and Eq.

7 gives the values of  $2a$  which differs from each other within less than 1%. Therefore for the evaluation of the zone of the ejecta destruction can be used relation Eq. 7, whereas for the local kinetic energy, relation Eq. 5. Dimensionless values for the average size of the destruction zone of ejecta  $2a/(2\pi r)$  are presented in Tab. 2 for different ejecta velocities  $V_0$ . The number of jets is estimated as  $n \approx \pi r / a$ .

In shot 7 (Tab. 1b), for which the number of deep channels in the collector is 21, the number of formed jets can also be taken as  $n=21$ . Tab. 7 shows that for assuming that the velocity of ejecta is equal to the impact velocity (2.7km/s) the evaluated number of jets ( $n=19$ ) is close to the experimental value.

## 5. CONCLUSIONS

The experiments reveal the following:

1. The spatial distribution of particles in an ejecta cone produced by an impact against an aluminum sheet may be considerably inhomogeneous because of formation of individual jets the concentration of material in which is considerably higher. The trajectories of the jets can be traced by the long narrow channels they produce in the polystyrene foam collectors.
2. The angle of escape of ejecta particles from a target surface depends on its thickness.
3. The mass of particles ejected from aluminum sheets exceeds sufficiently the case of mesh and multiple-mesh bumpers
4. The experiment results are consistent with presented model of ejecta destruction

## 6. ACKNOWLEDGEMENTS

This work was supported by ISTC project 3412.

The authors are grateful to Mr. N.S.Blinov and Mr. V.G.Bulanov from FGUP GOSNIAS for their indispensable contribution.

## 7. REFERENCES

1. Grady, D.E. (1982). Local Inertial Effects in Dynamic Fragmentation. *J. Appl. Phys.* **53**, 322–325.
2. Glenn, L.A. & Chudnovsky, A. (1986). Strain-energy Effects on Dynamic Fragmentation. *J. Appl. Phys.* **59**, 1379–1380.
3. Grady, D.E. (1988). The Spall Strength of Condensed Matter. *J. Mech. Phys. Solids* **36**, 353-384.

Table 1a. Shots data

Shot	Velocity, (km/s)	Target, (mm)	Target areal density, (kg/m <sup>2</sup> )	Weight of recovered substance (g)
1	2,23	alum.(D16) plate, 1.45	3,97	0,0656
2	2,65	alum.(AMG6) plate, 1.45	3,88	0,0781
3	2,66	alum.(AMG6) plate, 1.45	3,88	0,0549
4	2,64	3 steel meshes 1.0x0.32	2,82	0,0187
5	2,52	3 steel meshes 1.0x0.32	2,82	0,0154
6	3,19	3 steel meshes 1.0x0.32	2,82	0,0166

Table 1b. Shots data

Shot	Velocity, (km/s)	Target, (mm)	Weight of the target (kg/m <sup>2</sup> )
7	2,70	alum.(AMG6) plate, 3.00	8,10
8	2,83	alum.(AMG6) plate, 3.00	8,10

Table 2. Weight of recovered particles (shot 1)

Sector	Frontal part, (g.)	Rear part, (g.)	Total, (g.)	Number of particles with size bigger than 0.5 mm
1	0.0076	0.0047	0.0123	20
2	0.0017	0.0008	0.0025	8
3	0.0077	0.0077	0.0155	18
4	0.0074	0.0079	0.0153	14
5	0.0059	0.0064	0.0123	14
6	0.0058	0.0020	0.0077	12
<b>Total:</b>	<b>0.0361</b>	<b>0.0295</b>	<b>0.0656</b>	<b>86</b>

Table 3. Parameters of ejecta trajectories (see Fig. 7)

Channel I	Channel II	d <sub>b</sub> (mm)	d <sub>c</sub> (mm)	α <sub>I</sub>	α <sub>II</sub>	φ <sub>I</sub>	φ <sub>II</sub>	φ <sub>I</sub> + φ <sub>II</sub>
8	9	21	87	60	55	30	35	65
9	14	15.5	86.5	51.5	58.5	38.5	31.5	70
17	18	16	86	55	54.5	35	35.5	70.5
2	7	10.5	83	56	52	34	38	72
14	15	14	89.5	51	55	39	35	74
7	21	7	88	47.5	57.5	42.5	32.5	75
19	20	8	87	48	53	42	37	79
5	6	13	100	52	48	38	42	80
12	16	12	101	51	46.5	39	43.5	82.5
5	10	6	97	48	47	42	43	85
6	11	4	100	47	47	43	43	86

Table 4. Material parameters

Material	ρ, kg/m <sup>3</sup>	c <sub>0</sub> , m/s	E, GPa	K <sub>C</sub> , MPa, m <sup>1/2</sup>	σ*, MPa	Y, MPa	δ <sub>i</sub>
Aluminum alloy AMg6M	2.64·10 <sup>3</sup>	6.2·10 <sup>3</sup>	72	69	340	170	0.17

Table 5. Estimate results

Ejection velocity V <sub>0</sub> , km/s	a/πr, Relation Eq. 7	a/πr, Relation Eq. 5	Number of jets, n
0.5	0.159	0.161	~6
1.0	0.100	0.101	~10
2.0	0.063	0.063	~16
2.7	0.052	0.052	~19